APPENDIX

In this Appendix, the pairs of random variables $\{(\rho_u, \delta_u)|u \in \bigcup_{n=1}^{U} \mathcal{I}_{m^\star,n}, T^\star = N_t\}$ are proven to be i.i.d. To simplify the notation, define the set

$$\mathcal{C} := \left\{(\rho_u, \delta_u)|u \in \bigcup_{n=1}^{U} \mathcal{I}_{m^\star,n}, T^\star = N_t\right\} \overset{(a)}{=} \left\{(\rho_u, \delta_u)|u \in \bigcup_{n=1}^{U} \mathcal{I}_{m^\star,n}, |\mathcal{I}_{m^\star,n}| \geq 1 \forall\ 1 \leq n \leq N_t\right\}$$

where (a) follows from the definition of $T^\star$ in (1). Consider an index $a \in \mathcal{I}_{m^\star,k}$. By using Bayes' rule, the PDF of $\mathcal{C}$ defined before can be written as

$$\begin{aligned} f(\mathcal{C}) &= f\left((\rho_a, \delta_a)|a \in \mathcal{I}_{m^\star,k}, |\mathcal{I}_{m^\star,k}| \geq 1, \mathcal{C}/\{(\rho_a, \delta_a)\}\right) \times f\left(\mathcal{C}/\{(\rho_a, \delta_a)\}\right) \\ &\overset{(b)}{=} f\left((\rho_a, \delta_a)|a \in \mathcal{I}_{m^\star,k}, |\mathcal{I}_{m^\star,k}| \geq 1\}\right) \times f\left(\mathcal{C}/\{(\rho_a, \delta_a)\}\right) \\ &\overset{(c)}{=} f\left((\rho_a, \delta_a)|\rho_a \geq \gamma, \delta_a \leq \epsilon\right) \times f\left(\mathcal{C}/\{(\rho_a, \delta_a)\}\right) \end{aligned} \tag{11}$$

where (b) results from the fact that multiuser channels are independent and, thus, (ρ_a, δ_a) are independent of $\mathcal{C}/\{(\rho_a, \delta_a)$. The equality (c) follows from the definition in [1, (6)]. By repeatedly applying Bayes' rule using (11)

$$f(\mathcal{C}) = \prod_{n=1}^{N} \prod_{a \in \mathcal{I}_{m^\star,n}} f\left((\rho_a, \delta_a)|\rho_a \geq \gamma, \delta_a \leq \epsilon\right). \tag{12}$$

Since the multiuser channels are identically distributed ([1, Assumption 1]), $(\rho_u, \delta_u)\ \forall\ u$ follow the same distribution. Let (ρ, δ) denote a pair of random variables having the same distribution as (ρ_u, δ_u) for an arbitrary index u. Thus, (12) can be rewritten as

$$f(\mathcal{C}) = \left[f\left((\rho, \delta)|\rho \geq \gamma, \delta \leq \epsilon\right)\right]^{|\mathcal{C}|}. \tag{13}$$

The desired result follows from the aforementioned equation.

REFERENCES

[1] K. Huang, R. W. Heath, Jr., and J. G. Andrews, "SDMA with a sum feedback rate constraint," *IEEE Trans. Signal Process.*, vol. 55, no. 7, pp. 3879–3891, Jul. 2007.

[2] M. Sharif and B. Hassibi, "On the capacity of MIMO broadcast channels with partial side information," *IEEE Trans. Inf. Theory*, vol. 51, no. 2, pp. 506–522, Feb. 2005.

[3] K. Huang, R. W. Heath, Jr., and J. G. Andrews, "Joint beamforming and scheduling for SDMA systems with limited feedback," *IEEE Trans. Commun.*, Jun. 2006, submitted for publication.

A Jump Markov Particle Filter for Localization of Moving Terminals in Multipath Indoor Scenarios

M. Nicoli, *Member, IEEE*, C. Morelli, and V. Rampa

***Abstract*—This correspondence describes an efficient Bayesian framework for localization of moving terminals (MTs) in wideband wireless networks. In a previous paper, the authors have presented a grid-based technique, based on a hidden Markov model, that used the power delay profiles of the received signals to track the MT position. This grid-based Bayesian method has proved its efficacy in reducing localization errors in realistic indoor environments with multipath effects and mixed line-of-sight/non-line-of-sight (LOS/NLOS) conditions. However, the computational power and the memory storage requirements limit its use in practical wireless networks. To improve the computational efficiency, here we propose a jump-Markov particle-filter approach as an extension of the previous work; the LOS/NLOS sight process is the jumping feature that drives the MT motion dynamics, while the particle filter is used to track the MT position. Performance analyses, carried out for realistic multipath indoor environments, show that, with respect to the previous grid-based algorithm, this novel approach greatly reduces the tracking filter complexity still preserving the same localization accuracy. Simulation results prove also the robustness of the proposed method with respect to the uncertainty of sight statistics information.**

***Index Terms*—Bayesian estimation, hidden Markov model, mobile positioning, particle filter, source localization, tracking algorithms, ultra-wideband communications.**

I. INTRODUCTION

For a long time, ultra-wideband (UWB) systems have been used in radar and military applications for their improved signal resolution and power spectrum characteristics [1]. In recent years, they have been considered by the Federal Communications Commission for unlicensed-band applications, generating a lot of interest that has been supported also by the IEEE 802.15 personal area network standardization group. New applications, such as logistics, safety, environmental monitoring, require transparent radio localization. In environments covered by wireless networks, this task can be carried out by exploiting different type of measurements [2], [3]: times of arrival (TOA), time differences of arrival (TDOA), angles of arrival (AOA), and received signal strength (RSS). In particular, UWB short-range localization based on TOA/TDOA observations offers advantages in terms of positioning accuracy with respect to other narrowband systems [4], [5].

Manuscript received June 24, 2007; revised December 23, 2007. The associate editor coordinating the review of this manuscript and approving it for publication was Dr. Chong-Meng Samson See. This work was partially supported by the FIRB INSYEME project of the MIUR-FIRB Integrated System for Emergency (InSyEme) project under the Grant RBIP063BPH.

M. Nicoli is with the Dipartimento di Elettronica e Informazione, Politecnico di Milano, I-20133 Milan, Italy (e-mail: nicoli@elet.polimi.it).

C. Morelli was with the Dipartimento di Elettronica e Informazione, Politecnico di Milano, I-20133 Milan, Italy. He is now with Nokia Siemens Networks S.p.A., I-20060 Cassina de'Pecchi, Milan, Italy (e-mail: carlo.morelli@gmail.com).

V. Rampa is with the Institute of Electronics, Information and Telecommunications Engineering—National Research Council (I.E.I.I.T.—C.N.R.), I-20133 Milan, Italy (e-mail: rampa@elet.polimi.it).

Color versions of one or more of the figures in this paper are available online at http://ieeexplore.ieee.org.

Digital Object Identifier 10.1109/TSP.2008.920145

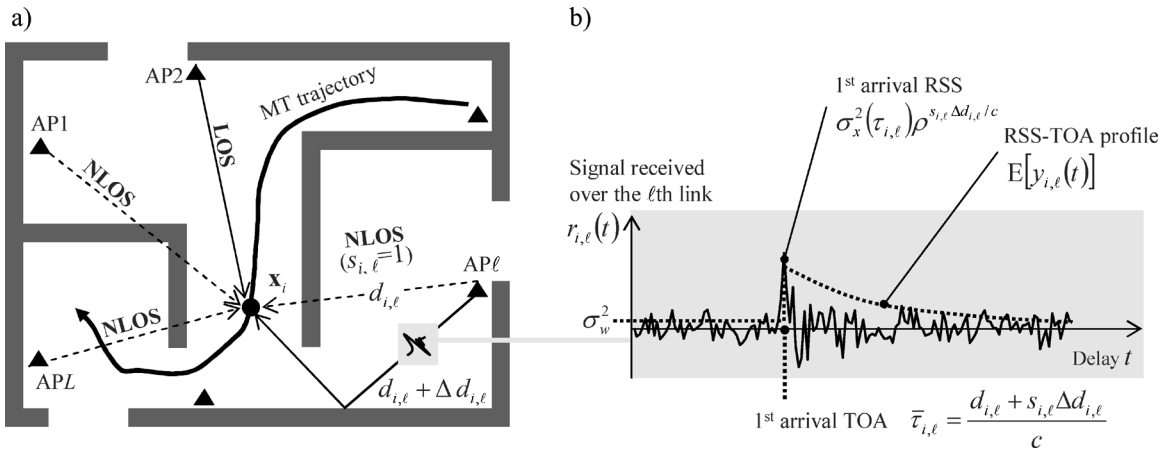

Fig. 1. Example of localization of a MT in mixed LOS/NLOS conditions: (a) indoor scenario and (b) signal received over the ℓth link.

In this correspondence, we propose an extension of a previous work [6] where a UWB infrastructure has been considered for tracking mobile terminals (MTs) in realistic indoor environments. A Bayesian filter based on RSS-delay profile observations has been introduced therein to exploit the high resolution of the UWB signal even in presence of multipath effects and mixed line-of-sight/non-line-of-sight (LOS/NLOS) conditions. This method uses a hidden Markov model (HMM) to describe the dynamics of the MT location and the evolution of the sight conditions with respect to the access points (APs), and a grid-based filter (GF) to jointly track them. Performance analyses in [6] have demonstrated the ability of this method in reducing localization errors with respect to local methods based on maximum-likelihood multi-lateration. However, the computational power and the memory storage requirements of the GF approach limit its use to complex and expensive network-based localization systems only. On the contrary, here we are interested in terminal-oriented real-time localization systems based on simple and inexpensive hardware devices. To accomplish this task, we propose an extension of the GF algorithm based on the following new features: a jump Markov system (JMS) [7] that jointly describes the MT dynamics and the sight-condition evolution, and a particle filter (PF) [8] that efficiently tracks the position of the moving target. In [9], an experimental study on wireless sensor networks has already proved the PF approach effectiveness (without JMS) for localization based on scalar RSS measurements (instead of RSS-versus-delay measurements). Here, PF is applied for the first time to *joint* RSS-delay measurements in a wideband wireless infrastructure with mixed LOS/NLOS conditions.

The use of PF for JMS state estimation has been previously investigated in [10] and [11] for target tracking. In this paper, we propose a new application for the localization of moving terminals in UWB networks with mixed LOS/NLOS conditions. Performance analyses, carried out in realistic multipath indoor environments, show that the joint use of JMS (to handle the sight conditions) and PF (to track the MT location) is an effective approach for radio localization in time dispersive UWB systems. Furthermore, since the statistics of LOS/NLOS conditions are usually unknown in practical applications, this paper investigates the robustness of the proposed method in case of uncertainty on the sight condition probabilities' knowledge. To summarize, the original contributions with respect to the previous work [6] and to other localization methods in the literature are as follows: the use of a JMS model to separate location and sight dynamics (instead of dealing with the joint location-sight state as in [6]); the introduction of the PF approach for a more efficient position sampling (compared to GF [6]) for localization from raw power-versus-delay UWB measurements; and the robustness analysis with respect to the uncertainty on sight condition statistics information.

The correspondence is organized as follows. The localization model is discussed in Section II, where signal measurements and network models are proposed. Section III introduces the JMS Bayesian framework and the PF tracking algorithms, whose performances are studied in Section IV in realistic LOS/NLOS indoor environments and compared with the GF ones. Finally, Section V draws some conclusions.

II. Problem Definition

We consider the terminal-oriented indoor localization scenario sketched in Fig. 1(a): An MT moves within an UWB infrastructured area $\mathcal{Q} \subset \mathbb{R}^2$ and it estimates its position using the signals received from $L \geq 3$ fixed APs. The APs are assumed to be placed in known positions and to be perfectly synchronized so that estimated delays can be used for ranging and combined by multilateration. In our framework, at the ith time instant, for $i = 1, \ldots, I$, the MT is characterized not only by the unknown spatial position $\mathbf{q}_i = [q_{i,1}, q_{i,2}] \in \mathcal{Q}$, but also by the unknown sight conditions $\mathbf{s}_i = [s_{i,1} \cdots s_{i,L}] \in \mathcal{S}$ computed with respect to the L known AP positions $\{\mathbf{q}_{\mathrm{AP}}^{(\ell)}\}_{\ell=1}^{L}$, with $\mathbf{q}_{\mathrm{AP}}^{(\ell)} \in \mathcal{Q}$. Each sight condition is represented by a binary random variable $s_{i,\ell}$, with value $s_{i,\ell} = 0$ for LOS and $s_{i,\ell} = 1$ for NLOS situations. The set $\mathcal{S} = \{0,1\}^L$ collects all the possible L-tuples of the LOS/NLOS binary variables. To simplify the analysis, we will assume that each sight condition $s_{i,\ell}$ evolves with the time i according to a dynamic system that is independent of the position $\mathbf{q}_i$ and of the other AP's sight conditions $\{s_{i,k}\}_{k \neq \ell}$.

A. Signal Model

We briefly recall here the UWB signal model introduced in [6]; the interested reader can refer to this paper for further details. At the ith time instant, the real-valued discrete-time signal received over the ℓth MT–AP link is modeled as the sum of two independent real-valued zero-mean white Gaussian signals:

$$r_{i,\ell}(t) = x_{i,\ell}(t) + w_{i,\ell}(t) \tag{1}$$

where $t \in \mathcal{T} = \{0, \Delta t, 2\Delta t, \ldots, (K-1)\Delta t\}$ denotes the time variable sampled with sampling interval Δt while K is the number of samples. The first term $x_{i,\ell}(t)$ in (1) represents the wideband signal propagated over a dense multipath channel linking $\mathbf{q}_{\mathrm{AP}}^{(\ell)}$ to $\mathbf{q}_i$, while $w_{i,\ell}(t)$ is an additive white Gaussian noise with mean power $\mathrm{E}[w_{i,\ell}^2(t)] = \sigma_w^2$. The multipath signal $x_{i,\ell}(t)$ is modeled as a non-stationary Gaussian random process having instantaneous power $y_{i,\ell}(t) = r_{i,\ell}^2(t)$ that

varies along the delay axis t according to an exponential power delay profile (PDP), as shown in the example of Fig. 1(b). The mean power is assumed to be

$$\mathrm{E}\left[y_{i,\ell}(t)\right] = \begin{cases} \sigma_w^2, & t < \bar{\tau}_{i,\ell} \\ \sigma_w^2 + \sigma_x^2(\tau_{i,\ell})\rho^{t-\tau_{i,\ell}}, & t \geq \bar{\tau}_{i,\ell}. \end{cases} \quad (2)$$

This PDP depends on the following quantities (see Fig. 1): the delay $\bar{\tau}_{i,\ell}$ and the power $\sigma_x^2(\tau_{i,\ell})$ of the first arrival; the multipath delay spread τ_{rms} or, equivalently, the PDP attenuation factor $\rho = \exp(-1/\tau_{rms}) \leq 1$ [12]. Notice that the first-arrival delay $\bar{\tau}_{i,\ell}$ is proportional to the MT–AP distance $d_{i,\ell} = |\mathbf{q}_i - \mathbf{q}_{\mathrm{AP}}^{(\ell)}|$ only in case of LOS ($s_{i,\ell} = 0$), as it equals the direct-path delay $\tau_{i,\ell} = d_{i,\ell}/c$ where c is the propagation velocity. On the other hand, in case of NLOS ($s_{i,\ell} = 1$), the propagation time is increased by the excess delay $\Delta\tau_{i,\ell} > 0$, as shown in the example of Fig. 1(b):

$$\bar{\tau}_{i,\ell} = \tau_{i,\ell} + s_{i,\ell} \cdot \Delta\tau_{i,\ell} = \frac{d_{i,\ell}}{c} + s_{i,\ell} \cdot \Delta\tau_{i,\ell}. \quad (3)$$

The NLOS excess delay $\Delta\tau_{i,\ell}$ is assumed to be a random variable with known distribution $f_{\Delta\tau}(\Delta\tau)$ [12]. Moreover, the first-arrival power $\sigma_x^2(\tau_{i,\ell})$ depends on the MT–AP distance, as it is ruled by the path-loss law [2]–[12]:

$$\sigma_x^2(\tau_{i,\ell}) = \sigma_{\mathrm{ref}}^2 \left(\frac{\tau_{\mathrm{ref}}}{\tau_{i,\ell}}\right)^{\alpha} = \sigma_{\mathrm{ref}}^2 \left(\frac{d_{\mathrm{ref}}}{d_{i,\ell}}\right)^{\alpha} \quad (4)$$

where σ_{ref}^2 is the power received at the reference distance $d_{\mathrm{ref}} = c\tau_{\mathrm{ref}}$ and α is the path-loss exponent (typical values are in the range $\alpha \in [2, 4]$). The signal-to-noise ratio (SNR) at the reference distance d_{ref} is defined as $\eta_{\mathrm{ref}} = (\sigma_{\mathrm{ref}}^2/\sigma_w^2)$.

Both the first-arrival delay (3) and the RSS (4) depend on the distance $d_{i,\ell}$ and thus they are functions of the position $\mathbf{q}_i$ (note that both functions are *nonlinear*, as the delay depends linearly on the distance but nonlinearly on the position). Thereby, we may select the complete PDP of the received signal vector, $\mathbf{y}_{i,\ell} = [y_{i,\ell}(0) \cdots y_{i,\ell}((K-1)\Delta t)]$ [see the example in Fig. 1(b)], as measurement for our Bayesian localization framework. Such a measurement may be considered as a *joint* observation of delay *and* power. The complete measurement set $\mathbf{y}_i = [\mathbf{y}_{i,1} \cdots \mathbf{y}_{i,L}]^T$ includes all the KL samples collected by the L APs at time i and modeled as described above.

III. Bayesian Tracking

In this section, we design a real-time state-space technique to estimate $\mathbf{q}_i$ every time a new observed set of signals $\mathbf{y}_i$ becomes available. The MT motion is modeled as a first-order HMM whose state $\mathbf{q}_i$ is hidden into the measurement $\mathbf{y}_i$. This dynamic model is used together with the measurement model defined in Section II-A to compute the optimal Bayesian estimate of $\mathbf{q}_i$. However, the statistics of the observed signal $\mathbf{y}_i$ change over the time due to the variations of the LOS/NLOS variable $\mathbf{s}_i$. In such a scenario, optimal estimation of the state $\mathbf{q}_i$ requires the definition of an additional dynamic model that describes the evolution of the sight state $\mathbf{s}_i$. This leads to a composite dynamic model having as state the *joint* sight-position variable $\mathbf{x}_i = (\mathbf{q}_i, \mathbf{s}_i)$ with $\mathbf{x}_i \in \mathcal{X} = \mathcal{Q} \times \mathcal{S}$.

The composite localization model is formulated in Section III-A as a jump Markov system [7]. This is defined as an HMM where the state and/or the measurement models depend on a driving Markov chain called the jumping feature. Following our assumptions, in the particular case herein considered, only the measurement model ($\mathbf{y}_i$) depends on the jumping feature ($\mathbf{s}_i$): in fact, the probability density function (pdf) of the measurement $\mathbf{y}_i$ is driven by the discrete process $\mathbf{s}_i$, while the state $\mathbf{q}_i$ is assumed to be independent of $\mathbf{s}_i$. Once the JMS has been defined, the evolution of the sight-position state $\mathbf{x}_i$ can be tracked by means of a Bayesian filter, as described in Section III-B.

A. JMS Dynamic Model

The Markov models describing the location and sight dynamics are defined according to [6], as briefly recalled in this paragraph. The MT location $\mathbf{q}_i$ is modeled as a first-order Markov process ruled by the system equation $\mathbf{q}_i = \mathbf{q}_{i-1} + \mathbf{v}_i$, where $\mathbf{v}_i \in \mathcal{Q}$ is the motion driving process with known distribution $f_{\mathbf{v}}(\mathbf{v}_i)$ (this can be, in general, *non-Gaussian*, as in the examples given in [6] and in the localization scenario simulated in Section IV). The motion transition probabilities are then given by $p(\mathbf{q}_i|\mathbf{q}_{i-1}) = f_{\mathbf{v}}(\mathbf{q}_i - \mathbf{q}_{i-1})$. In the same way, each jumping variable $s_{i,\ell}$ is modeled as a binary Markov chain described by a 2×2 transition probability matrix [6] which is completely defined by the couple of transition probabilities $P(s_{i,\ell} = 0|s_{i-1,\ell} = 0) = p_0$ and $P(s_{i,\ell} = 1|s_{i-1,\ell} = 1) = p_1$. Under the assumption of independence between the L MT–AP links, the whole sight process $\mathbf{s}_i$ is a first-order Markov chain with transition probabilities $P(\mathbf{s}_i = \mathbf{k}|\mathbf{s}_{i-1} = \mathbf{h}) = \prod_{\ell=1}^{L} P(s_{i,\ell} = k_\ell|s_{i-1,\ell} = h_\ell)$, for $\mathbf{k} = [k_1 \cdots k_L]$, $\mathbf{h} = [h_1 \cdots h_L] \in \mathcal{S}$. The transition pdf from the position-sight state $\mathbf{x}_{i-1} = (\mathbf{q}_{i-1}, \mathbf{s}_{i-1})$ to the next one $\mathbf{x}_i = (\mathbf{q}_i, \mathbf{s}_i)$ is finally given by $p(\mathbf{x}_i|\mathbf{x}_{i-1}) = p(\mathbf{q}_i|\mathbf{q}_{i-1})P(\mathbf{s}_i|\mathbf{s}_{i-1})$. The initial state distribution $p(\mathbf{x}_0) = p(\mathbf{q}_0)P(\mathbf{s}_0)$ can be chosen according to the available *a priori* information about the position $\mathbf{q}_0$ and the sight $\mathbf{s}_0$ at the starting time.

The JMS position-sight state $\mathbf{x}_i$ is hidden into the L-link observation vector $\mathbf{y}_i$ composed by the conditionally independent measurements $\{\mathbf{y}_{i,\ell}\}_{\ell=1}^{L}$. The conditioned pdf of the observation is thus $p(\mathbf{y}_i|\mathbf{x}_i) = \prod_{\ell=1}^{L} p(\mathbf{y}_{i,\ell}|\mathbf{q}_i, s_{i,\ell})$, where each pdf $p(\mathbf{y}_{i,\ell}|\mathbf{q}_i, s_{i,\ell})$ has to be evaluated according to the signal model in Section II-A. Here, we have selected as measurements the power samples $y_{i,\ell}(t)$ instead of the Gaussian signals $r_{i,\ell}(t)$ as described in [6]. Thereby, $\mathbf{y}_{i,\ell}$ is a vector of K independent chi-square variables with one degree of freedom. When conditioned to a given position $\mathbf{q}_i$ and a sight value $s_{i,\ell}$ (i.e., to the geometrical distance $d_{i,\ell} = |\mathbf{q}_i - \mathbf{q}^{(\ell)}|$, the LOS delay $\tau_{i,\ell} = d_{i,\ell}/c$ and the first-arrival delay $\bar{\tau}_{i,\ell} = \tau_{i,\ell} + s_{i,\ell} \cdot \Delta\tau_{i,\ell}$), the mean values, and thus the pdfs, of the chi-square variables are completely defined by (2). For the two LOS/NLOS sight cases, the conditioned pdf can be written as

$$\begin{aligned} p(\mathbf{y}_{i,\ell}|\mathbf{q}_i, s_{i,\ell} = 0) &= p\left(\mathbf{y}_{i,\ell}|\tau_{i,\ell} = \left|\mathbf{q}_i - \mathbf{q}^{(\ell)}\right|/c, \bar{\tau}_{i,\ell} = \tau_{i,\ell}\right) \\ &= \Lambda\left(\mathbf{y}_{i,\ell}, \left|\mathbf{q}_i - \mathbf{q}^{(\ell)}\right|/c, 0\right), \\ p(\mathbf{y}_{i,\ell}|\mathbf{q}_i, s_{i,\ell} = 1) &= \sum_{\Delta\tau} p\left(\mathbf{y}_{i,\ell}|\tau_{i,\ell} = \left|\mathbf{q}_i - \mathbf{q}^{(\ell)}\right|/c, \right. \\ &\qquad \left. \bar{\tau}_{i,\ell} = \tau_{i,\ell} + \Delta\tau\right) f_{\Delta\tau}(\Delta\tau) \\ &= \sum_{\Delta\tau} \Lambda\left(\mathbf{y}_{i,\ell}, \left|\mathbf{q}_i - \mathbf{q}^{(\ell)}\right|/c, \Delta\tau\right) f_{\Delta\tau}(\Delta\tau) \end{aligned}$$

where $\Lambda(\mathbf{y}, \tau, \Delta\tau)$ is the pdf of a generic $K \times 1$ signal vector $\mathbf{y} = [y(0) \cdots y((K-1)\Delta t)]^{\mathrm{T}}$, modeled as in Section II-A, with LOS delay τ, first-arrival delay $\tau + \Delta\tau$ and NLOS additional delay $\Delta\tau$ having pdf $f_{\Delta\tau}(\Delta\tau)$. Let $\phi(y) = \exp(-y/2)/\sqrt{2\pi y}$ be the pdf of a chi-square random variable with one degree of freedom and mean value $\mathrm{E}[y] = 1$, from the above considerations the pdf of $\mathbf{y}$ is the product of K chi-square pdfs having mean values (2):

$$\Lambda(\mathbf{y}, \tau, \Delta\tau) = \prod_{t<\tau+\Delta\tau} \frac{\phi\left(\frac{y(t)}{\sigma_w^2}\right)}{\sigma_w} \prod_{t\geq\tau+\Delta\tau} \frac{\phi\left(\frac{y(t)}{\sigma_w^2+\sigma_x^2(\tau)\rho^{t-\tau}}\right)}{\sqrt{\sigma_w^2 + \sigma_x^2(\tau)\rho^{t-\tau}}}. \quad (5)$$

B. Bayesian Filters

The *local* (i.e., without tracking) maximum-likelihood (LML) estimate of the state $\mathbf{x}_i$ can be obtained by applying the maximum-likelihood estimation criterion to the measurement $\mathbf{y}_i$: $\widehat{\mathbf{x}}_i^{\mathrm{LML}} = \arg\max_{\mathbf{x}_i \in \mathcal{X}} p(\mathbf{y}_i|\mathbf{x}_i)$. However, this *local* method is prone to localization errors and it should be avoided. On the other hand, an optimal estimate of $\mathbf{x}_i$ can be extracted from the *whole* set of measurements $\mathbf{y}_{1:i} = \{\mathbf{y}_1, \ldots, \mathbf{y}_i\}$ available at time i, by exploiting the dynamic model shown in Section III-A. This estimate is obtained by evaluating the *a posteriori* pdf $p(\mathbf{x}_i|\mathbf{y}_{1:i})$, which embodies all the statistical information that can be extracted from $\mathbf{y}_{1:i}$ about the state $\mathbf{x}_i$. According to the Bayes' rule, the *a posteriori* pdf depends on the conditioned pdf $p(\mathbf{y}_i|\mathbf{x}_i)$ and the *a priori* pdf $p(\mathbf{x}_i|\mathbf{y}_{1:i-1})$ as

$$p(\mathbf{x}_i|\mathbf{y}_{1:i}) \propto p(\mathbf{y}_i|\mathbf{x}_i)p(\mathbf{x}_i|\mathbf{y}_{1:i-1}). \tag{6}$$

For each $i > 0$, the *a priori* pdf can be computed by the Chapman–Kolmogorov equation [8] as

$$p(\mathbf{x}_i|\mathbf{y}_{1:i-1}) - p(\mathbf{q}_i, \mathbf{s}_i|\mathbf{y}_{1:i-1}) = \sum_{\mathbf{s}_{i-1} \in \mathcal{S}} P(\mathbf{s}_i|\mathbf{s}_{i-1}) \times \int_{\mathcal{Q}} p(\mathbf{q}_i|\mathbf{q}_{i-1})p(\mathbf{q}_{i-1}, \mathbf{s}_{i-1}|\mathbf{y}_{1:i-1})d\mathbf{q}_{i-1} \tag{7}$$

while, for $i = 1$, $p(\mathbf{x}_1|\mathbf{y}_0) = p(\mathbf{x}_1)$ can be obtained from (7) by setting $p(\mathbf{q}_{i-1}, \mathbf{s}_{i-1}|\mathbf{y}_{1:i-1}) = p(\mathbf{q}_0)P(\mathbf{s}_0)$.

The recursive computation of (6) and (7) yields the *a posteriori* pdf $p(\mathbf{x}_i|\mathbf{y}_{1:i})$ for any i; then, the optimal Bayesian estimate of the state $\mathbf{x}_i$ can be obtained from $p(\mathbf{x}_i|\mathbf{y}_{1:i})$ by using the maximum *a posteriori* (MAP) or the minimum mean-square error (MMSE) criterion. However, in the general case of non-Gaussian nonlinear dynamic systems, as the one considered in this paper, the *a posteriori* pdf cannot be determined analytically from (6), (7). Suboptimal algorithms are required, using the GF or the PF, in order to approximate the continuous state space by a discrete finite set and to reduce the evaluation of the *a posteriori* pdf to the computation of a finite set of probabilities.

1) Grid-Based Filter: Grid-based Bayesian methods rely on a uniform sampling of the continuous state space $\mathcal{X}$. For the specific localization problem herein considered, GF tracking can be obtained as proposed in [6], by quantizing the location space $\mathcal{Q}$ into a finite regular 2-D grid $\mathcal{Q}_{N_1 \times N_2}$ composed of $N_1 \times N_2$ bins. The overall state-space $\mathcal{X}$ reduces to the discrete finite set $\mathcal{X}_{N_g} = \{\mathbf{x}^{(n)}\}_{n=1}^{N_g}$ of $N_g = N_1 N_2 2^L$ states, each state being defined as $\mathbf{x}^{(n)} = (\mathbf{q}^{(n)}, \mathbf{s}^{(n)})$ with $\mathbf{q}^{(n)} \in \mathcal{Q}_{N_1 \times N_2}$ and $\mathbf{s}^{(n)} \in \mathcal{S}$. The pdf (6) is thus approximated by the finite sum

$$p(\mathbf{x}_i|\mathbf{y}_{1:i}) \approx \sum_{n=1}^{N_g} w_i^{(n)} \delta\left(\mathbf{q}_i - \mathbf{q}^{(n)}\right) \delta\left[\mathbf{s}_i - \mathbf{s}^{(n)}\right] \tag{8}$$

where $w_i^{(n)} = P(\mathbf{x}_i = \mathbf{x}^{(n)}|\mathbf{y}_{1:i})$ denotes the probability that $\mathbf{x}_i$ belongs to the nth bin given the measurements $\mathbf{y}_{1:i}$, while $\delta(\cdot)$ and $\delta[\cdot]$ represent the continuous and discrete Dirac's pulses, respectively. The *a posteriori* distribution $w_i^{(n)}$ can be calculated recursively through the update-prediction stages (6), (7) discretized as shown in [6, Eq. 38–40], with a computational complexity $\mathcal{O}(N_g)$ proportional to the grid size N_g ($\mathcal{O}(\cdot)$ stands for "in the order of"). The disadvantage of this approach is that the uniform grid must be dense enough to get high localization resolution, thus leading to unfeasible computational burden for practical real-time localization systems.

2) Particle Filter: The key idea of particle filtering [8] is to approximate the *a posteriori* pdf by a set of samples with associated weights as in (8), but with samples that are randomly distributed over the state space according to a given distribution (i.e., the importance density). Compared to the GF method, random sampling is a more efficient approach as it allows to concentrate the samples only where they are really needed (i.e., where the location probability is higher).

At first, let us approximate the *a priori* pdf $p(\mathbf{x}_i|\mathbf{y}_{1:i-1}) = p(\mathbf{q}_i, \mathbf{s}_i|\mathbf{y}_{1:i-1})$ as the sum of a large number of Dirac's pulses equally weighted and centered around N_p samples (or *particles*) $\{\mathbf{q}_i^{(n)}, \mathbf{s}_i^{(n)}\}_{n=1}^{N_p}$ with $\mathbf{q}_i^{(n)} \in \mathcal{Q}$ and $\mathbf{s}_i^{(n)} \in \mathcal{S}$. The N_p samples are independent and identically distributed (i.i.d.) random variables with distribution $p(\mathbf{q}_i, \mathbf{s}_i|\mathbf{y}_{1:i-1})$; this will be indicated in the following as: $(\mathbf{q}_i^{(n)}, \mathbf{s}_i^{(n)}) \sim p(\mathbf{q}_i, \mathbf{s}_i|\mathbf{y}_{1:i-1})$. The pdf approximation is

$$p(\mathbf{q}_i, \mathbf{s}_i|\mathbf{y}_{1:i-1}) \approx \frac{1}{N_p} \sum_{n=1}^{N_p} \delta\left(\mathbf{q}_i - \mathbf{q}_i^{(n)}\right) \delta\left[\mathbf{s}_i - \mathbf{s}_i^{(n)}\right]. \tag{9}$$

The particle subset $\{\mathbf{q}_i^{(n)}, \mathbf{s}_i^{(n)}\}_{n=1}^{N_p}$ is finite and discrete, but not deterministic and fixed as in the GF approach. In particular, each sight particle $\mathbf{s}_i^{(n)}$ is still defined on the finite and discrete set $\mathcal{S}$, but the location particle $\mathbf{q}_i^{(n)}$ can now potentially assume any (continuous) value in $\mathcal{Q}$. The *a posteriori* pdf can be similarly approximated using (6):

$$\begin{aligned} p(\mathbf{q}_i, \mathbf{s}_i|\mathbf{y}_{1:i}) &\propto p(\mathbf{y}_i|\mathbf{q}_i, \mathbf{s}_i)p(\mathbf{q}_i, \mathbf{s}_i|\mathbf{y}_{1:i-1}) \\ &\approx \frac{1}{N_p} \sum_{n=1}^{N_p} p(\mathbf{y}_i|\mathbf{q}_i, \mathbf{s}_i)\delta\left(\mathbf{q}_i - \mathbf{q}_i^{(n)}\right) \delta\left[\mathbf{s}_i - \mathbf{s}_i^{(n)}\right] \\ &= \sum_{n=1}^{N_p} \tilde{w}_i^{(n)} \delta\left(\mathbf{q}_i - \mathbf{q}_i^{(n)}\right) \delta\left[\mathbf{s}_i - \mathbf{s}_i^{(n)}\right] \end{aligned} \tag{10}$$

with *weight* $\tilde{w}_i^{(n)}$ defined as $\tilde{w}_i^{(n)} = p(\mathbf{y}_i|\mathbf{q}_i^{(n)}, \mathbf{s}_i^{(n)})/N_p$. Equality holds when normalization is introduced, i.e., for

$$p(\mathbf{q}_i, \mathbf{s}_i|\mathbf{y}_{1:i}) = \sum_{n=1}^{N_p} w_i^{(n)} \delta\left(\mathbf{q}_i - \mathbf{q}_i^{(n)}\right) \delta\left[\mathbf{s}_i - \mathbf{s}_i^{(n)}\right] \tag{11}$$

with $w_i^{(n)} = \tilde{w}_i^{(n)} / \sum_{m=1}^{N_p} \tilde{w}_i^{(m)}$. Here, the terms $w_i^{(n)}$ are different from those in (8); the same name has been retained to stress similarities between the GF and the PF approach. The main advantage of this approximation is that expectations of $\mathbf{q}_i$ and $\mathbf{s}_i$ are easily computed, being, for the generic function $f(\cdot)$: $\mathrm{E}[f(\mathbf{q}_i, \mathbf{s}_i)] \approx \sum_{n=1}^{N_p} w_i^{(n)} f(\mathbf{q}_i^{(n)}, \mathbf{s}_i^{(n)})$. It follows that the MMSE estimates can be calculated through the weighted means:

$$\hat{\mathbf{q}}_i^{\mathrm{PF}} = \sum_{n=1}^{N_p} w_i^{(n)} \mathbf{q}_i^{(n)} \tag{12}$$

$$\widehat{\mathbf{s}}_i^{\mathrm{PF}} = \mathrm{dec}\left(\sum_{n=1}^{N_p} w_i^{(n)} \mathbf{s}_i^{(n)}\right) \tag{13}$$

where $\mathrm{dec}(x) = 1$ for $x \geq 1/2$ and $\mathrm{dec}(x) = 0$ for $x < 1/2$.

At the $(i+1)$th time step, the *a priori* particle distribution $\{\mathbf{q}_{i+1}^{(n)}, \mathbf{s}_{i+1}^{(n)}\}_{n=1}^{N_p}$ is computed through the sequential importance resampling variant [8] of PF. At first, the current particles $\{\mathbf{q}_i^{(m)}, \mathbf{s}_i^{(m)}\}_{m=1}^{N_p}$ are resampled (either deterministically or randomly [8]) in a new set $\{\tilde{\mathbf{q}}_i^{(n)}, \tilde{\mathbf{s}}_i^{(n)}\}_{n=1}^{N_p}$ such that $P(\tilde{\mathbf{q}}_i^{(n)} = \mathbf{q}_i^{(m)}, \tilde{\mathbf{s}}_i^{(n)} = \mathbf{s}_i^{(m)}) = w_i^{(m)}, \forall n$. Through this resampling step, particles with negligible weight are dropped while particles with strong weight are dismantled in a set of particles with uniform values $\tilde{w}_i^{(n)} = 1/N_p$. The next step (forwarding step) consists in sampling the position and sight transition distributions according to the state equations, in order to obtain the new particle set: $\mathbf{q}_{i+1}^{(n)} = \tilde{\mathbf{q}}_i^{(n)} + \mathbf{v}_{i+1}^{(n)}$ with $\mathbf{v}_{i+1}^{(n)} \sim f_v(\mathbf{v}_{i+1})$ and $\mathbf{s}_{i+1}^{(n)} \sim P(\mathbf{s}_{i+1}) = \sum_{\mathbf{s}_i} P(\mathbf{s}_{i+1}|\mathbf{s}_i)P(\mathbf{s}_i)$, $\forall n$. At the first iteration, the particle distribution is sampled as $\mathbf{q}_0^{(n)} \sim p(\mathbf{q}_0)$ and $\mathbf{s}_0^{(n)} \sim P(\mathbf{s}_0), \forall n$. Please note that the overall

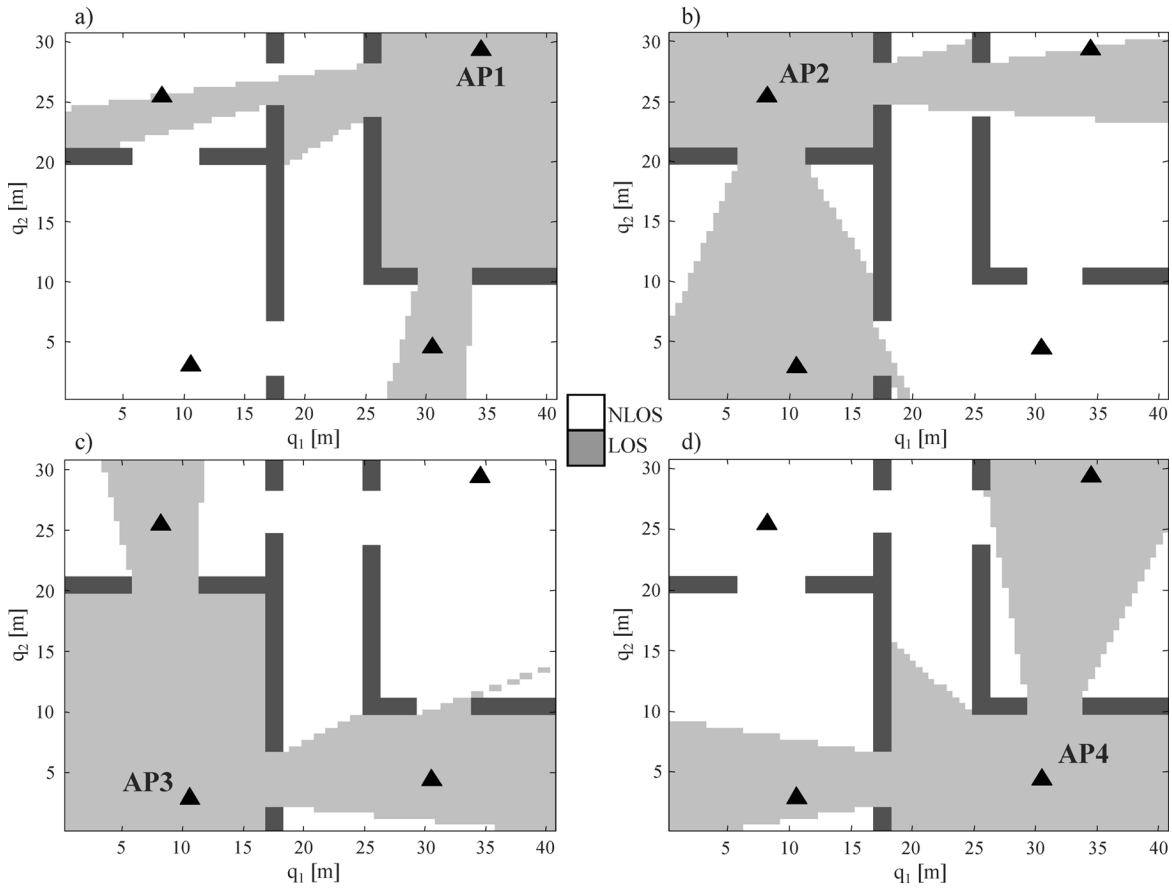

Fig. 2. Sight conditions $s_{i,\ell}$ for AP number $\ell = 1, 2, 3, 4$ and for MT position $\mathbf{q}_i$ ranging over the whole 2-D space $\mathcal{Q}$: Gray bins indicate LOS condition ($s_{i,\ell} = 0$), white bins NLOS ($s_{i,\ell} = 1$).

computational complexity $\mathcal{O}(N_p)$ required by the PF algorithm is linearly related to the number of particles N_p.

IV. Numerical Results

Positioning performances are assessed by simulating the localization scenario in Fig. 2: the MT, while moving within an indoor environment of 40 m × 30 m, is localized by means of an UWB infrastructure composed of $L = 4$ APs. Within the allowed 2-D space (walls and areas close to the APs are not permitted), the MT trajectory $\{\mathbf{q}_i\}_{i=1}^{I}$ is simulated according to the first-order HMM in Section III, using a *non-Gaussian* driving process $\mathbf{v}_i$ with conic-shaped pdf $f_{\mathbf{v}}(\mathbf{v})$ of base radius 2 m as the one shown in [6, Fig. 9(c)]. Sight conditions are generated by accessing the LOS/NLOS maps, shown in Fig. 2(a)–(d) for the four APs, according to the simulated MT trajectory. These coverage maps have been obtained by performing ray tracing from each MT position $\mathbf{q}_i \in \mathcal{Q}$ with respect to the AP positions $\{\mathbf{q}_{\mathrm{AP}}^{(\ell)}\}_{\ell=1}^{4}$: for each MT–AP link, the sight condition is set to $s_{i,\ell} = 1$ when the line linking the AP and the MT positions crosses a wall (NLOS), otherwise it is $s_{i,\ell} = 0$ (LOS). It can be noticed that most of the area is covered by only one AP (in the room corners) or, at most, two (along the strips connecting two APs) while the central part of the corridor is not covered at all. This makes the localization task particularly complicated and requires MT tracking in order to avoid large errors due to poor coverage. Furthermore, in this realistic scenario, position and sight are no longer independent, as, for any value of $\mathbf{q}_i$, the corresponding sight conditions are deterministically assigned by the layout geometry. Nevertheless, the Bayesian methods in Section III (based on the simplifying assumption of independence between position and sight) will be shown to provide good localization performances.

Measurements $\{\mathbf{y}_i\}_{i=1}^{I}$ are simulated according to the signal model (1)–(4), thereby they are *nonlinearly* related to the MT location $\mathbf{q}_i$. The received signal vector $\mathbf{y}_i$ is sampled at $f_s = 1/\Delta t = 1$ GHz and has length $K = 150$. For each position along the MT trajectory, the associated measurement is generated by evaluating the propagation time $\tau_{i,\ell}$ according to the layout geometry in Fig. 2. In case of NLOS, an additional delay $\Delta\tau_{i,\ell}$ is simulated using an exponential pdf $f_{\Delta\tau}(\Delta\tau) \propto \exp(-\Delta\tau/10\text{ ns})$ [12]. The signal power $\sigma_x^2(\tau_{i,\ell})$ is derived according to the path-loss law (4), assuming path-loss exponent $\alpha = 2.4$ and SNR $\eta_{\mathrm{ref}} = 40$ dB at the reference distance $d_{\mathrm{ref}} = 1$ m. Multipath components have exponential PDP with $\bar{\rho} = \exp(-\Delta t/\tau_{rms}) = 0.9$ ($\tau_{rms} = 10$ ns). All these parameters are assumed to be perfectly known by the localization algorithm.

The MT transition probabilities are assumed to be known for tracking. As far as the sight tracking is concerned, the values to be used for $\{p_0, p_1\}$ are drawn directly from the layout in Fig. 2 as follows. A training trajectory of $I = 2 \times 10^4$ steps is simulated across the considered layout. Then, the relative frequencies of transition from LOS to LOS (p_0) and from NLOS to NLOS (p_1) are evaluated by counting the two events occurrences along the MT trajectory for the four APs. The resulting frequencies, for the specific layout herein considered, yield $p_0 \approx p_1 \approx 0.9$ (under the assumption of transition probabilities equal for all the four APs and independent of the MT position). Notice that this approach for the estimation of p_0 and p_1 can always be used when the layout planimetry is known.

For the estimation of the MT trajectory, we compare the LML, GF and PF methods. MT tracking is implemented using the simplifying assumption of independence between sight and position and taking into account the locality of the MT motion (i.e., the fact that the probabilities

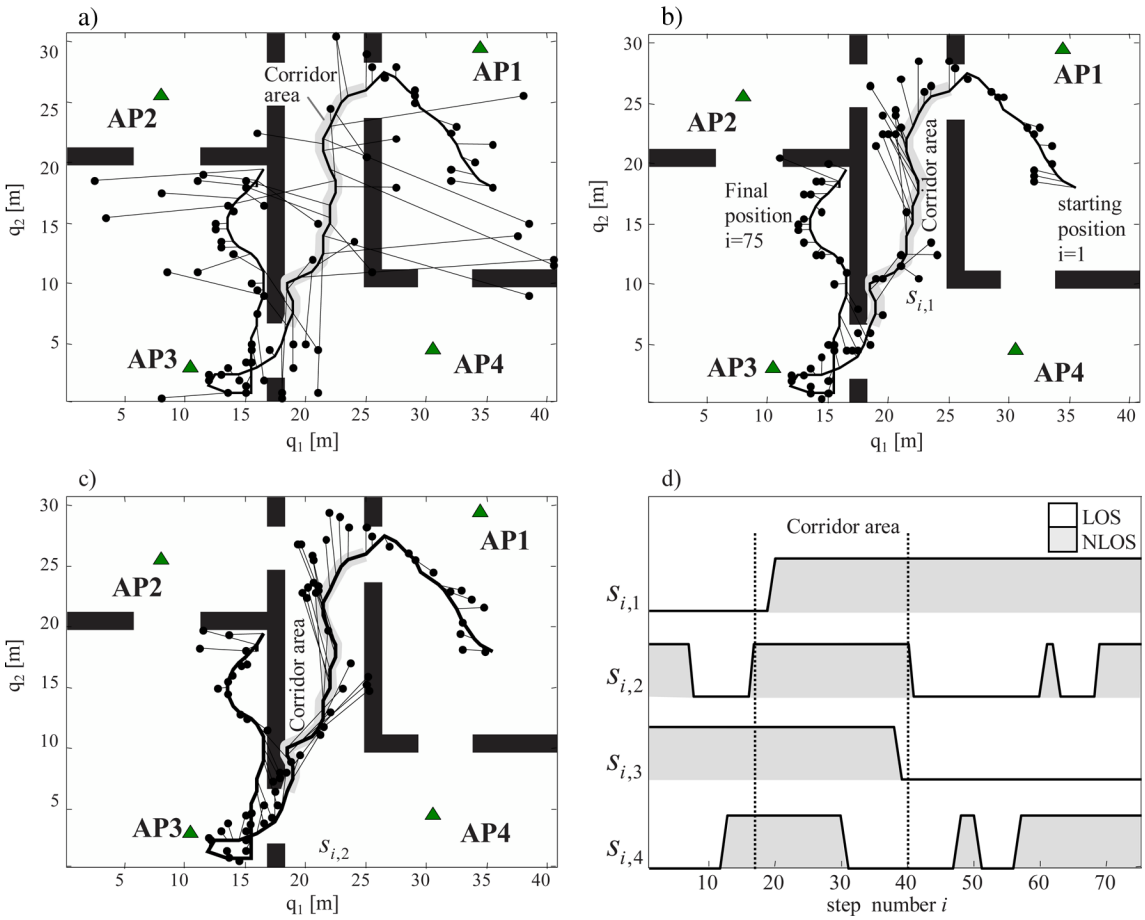

Fig. 3. Example of MT tracking: (a)–(c) localization by (a) LML, (b) GF and (c) PF; (d) sight conditions along the path with respect to all APs. Straight lines connecting dots to the MT trajectory indicate the localization errors for each algorithm along the MT path.

$p(\mathbf{q}_i|\mathbf{q}_{i-1})$ are non-null only within a circle of 2m radius centered on the position $\mathbf{q}_{i-1}$). The 2-D grid $\mathcal{Q}_{N_1\times N_2}$ used for GF tracking is composed of 81 × 61 bins (the spatial sampling interval is $\Delta q = 0.5$ m), thus leading to an overall number of discrete states $N_g = 81\cdot 61\cdot 2^4 \approx 7.9\times 10^4$. On the contrary, a much smaller number of particles is used for PF tracking: $N_p = 10^3 \ll N_g$.

A tracking example is shown in Fig. 3. Here, the MT path has been generated smoother and shorter $(I = 75)$ for visualization purposes only. This figure compares the true trajectory (thick line) with the estimated ones (markers) obtained by (a) LML estimate, (b) GF, and (c) PF. The localization errors can be appreciated by looking at the lines that connect the true and the estimated positions in Fig. 3(a)–(c). Sight conditions with respect to all APs are represented in Fig. 3(d) for each position of the MT along the path. It can be seen that, for position number $i = 16,\ldots,39$, almost all APs are shadowed by the corridor walls, thus leading to large localization errors.

For the same tracking example, Fig. 4 shows the 75 UWB signals received over each AP–MT link as the MT moves along the trajectory shown in Fig. 3. Looking at this trajectory, it can be noticed that the MT position is always far away from AP2 and AP4, while it gets closer to AP1/AP3 at the beginning/end of the MT path. Thereby, we expect the SNR experienced by AP2 and AP4 measurements to be particularly low, as it is indeed in the two plots on the right of Fig. 4. To allow a clear visualization of the measurement sets, notwithstanding the unbalanced SNR, in this figure, the measurements collected by AP1, AP2, and AP4 have been amplified by an amplitude factor equal to, respectively, 3, 7, and 6 (AP3 is the one with the higher SNR values). Gray background denotes NLOS condition, while the superimposed dashed and solid lines indicate the actual MT–AP range $d_{i,\ell}$ and the apparent one extracted from the first arrival LOS/NLOS delay $d_{i,\ell} + \Delta d_{i,\ell} = \bar{\tau}_{i,\ell}\cdot c$, respectively. The two lines differ when NLOS conditions occur: in this case the received UWB signal is highly attenuated and the background noise is dominant. On the other hand, the power of the first-arrival signal increases when the AP is not shadowed and it is close to the MT, such as for AP1 in Fig. 4(a) for $i = 1,\ldots,20$ and for AP3 in Fig. 4(c) for $i = 40,\ldots,60$.

For AP1 only, Fig. 5 shows the MT–AP distance $d_{i,1}$ (lines) and the corresponding estimate (markers) obtained by (a) LML, (b) GF, and (c) PF localization. The number of shadowed APs is given in Fig. 5(d) as a function of the position index i along the MT path. In all the four plots, gray areas are related to the position numbers i for which more than two APs are shadowed with respect to the MT. In these areas, the localization accuracy is poor, especially in the corridor for $i = 25,\ldots,38$ (see also the corridor localization results in Fig. 3); still, the NLOS bias is successfully compensated by the Bayesian tracking using the *a priori* information about the location dynamics and the excess delay statistics. In this example, the compensation in the corridor area is more effective for GF than PF, due to the moderate number of particles.In the rest of the path, both PF and GF have similar accuracy and they largely outperform LML localization. The estimate results in Fig. 5, compared to the biased range values (solid lines) in Fig. 4(a), highlight also the performance improvement that can be obtained with respect to conventional localization based on separate ranging and multilateration. In the NLOS area, separate ranging over the MT–AP1 link would give rise to higher estimation errors, as shown by the two diverging lines in Fig. 4(a).

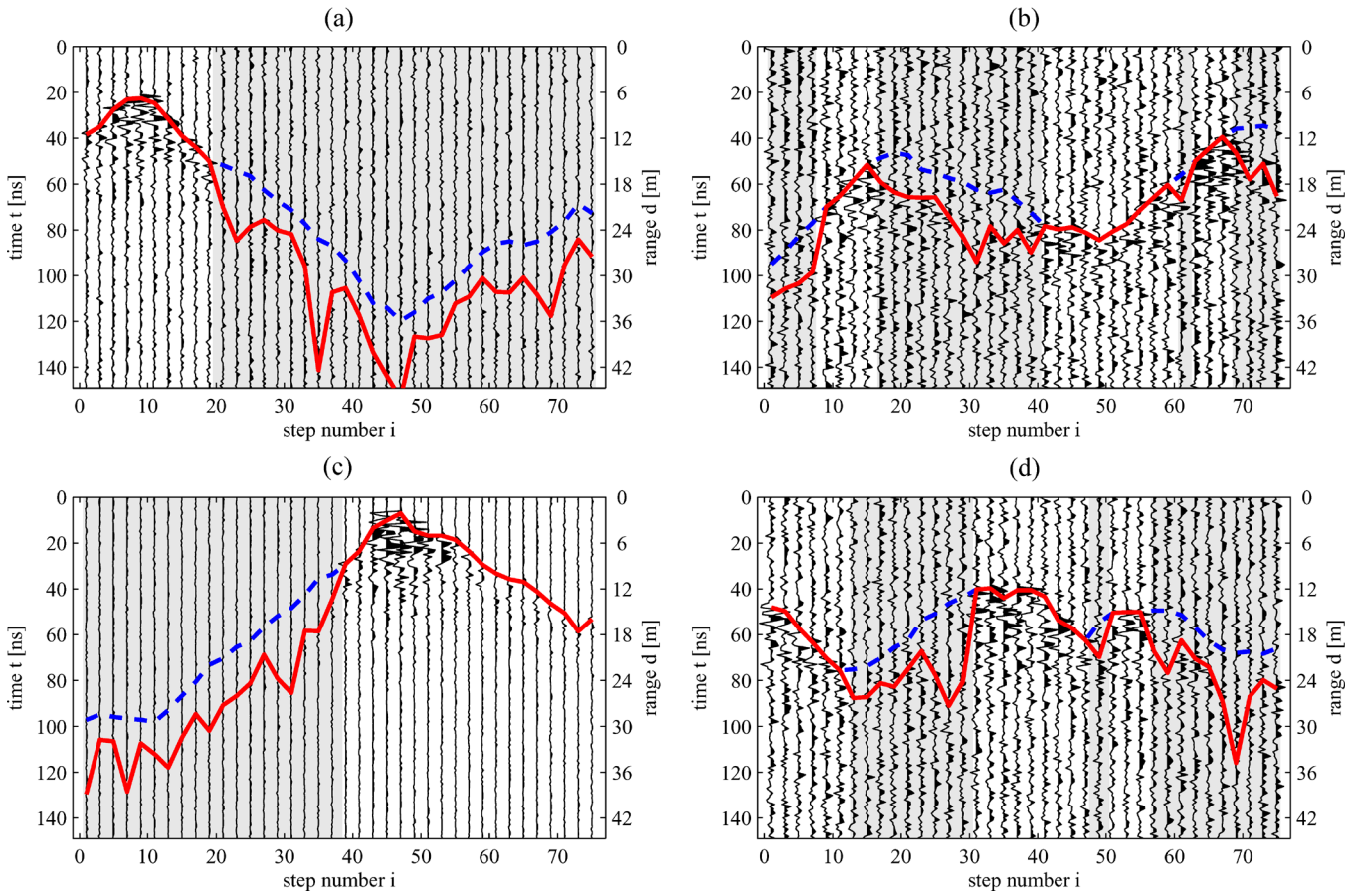

Fig. 4. UWB signals measured over the four AP–MT links as the MT moves along the path of length $I = 75$ in Fig. 3. Gray background denotes NLOS. Superimposed dashed and solid lines indicate the true MT–AP range and the apparent MT–AP range drawn from the first arrival delay, respectively. (a) $\mathrm{r_{i,1}(t)} \times 3$; (b) $\mathrm{r_{i,2}(t)} \times 7$; (c) $\mathrm{r_{i,3}(t)}$; (d) $\mathrm{r_{i,4}(t)} \times 6$.

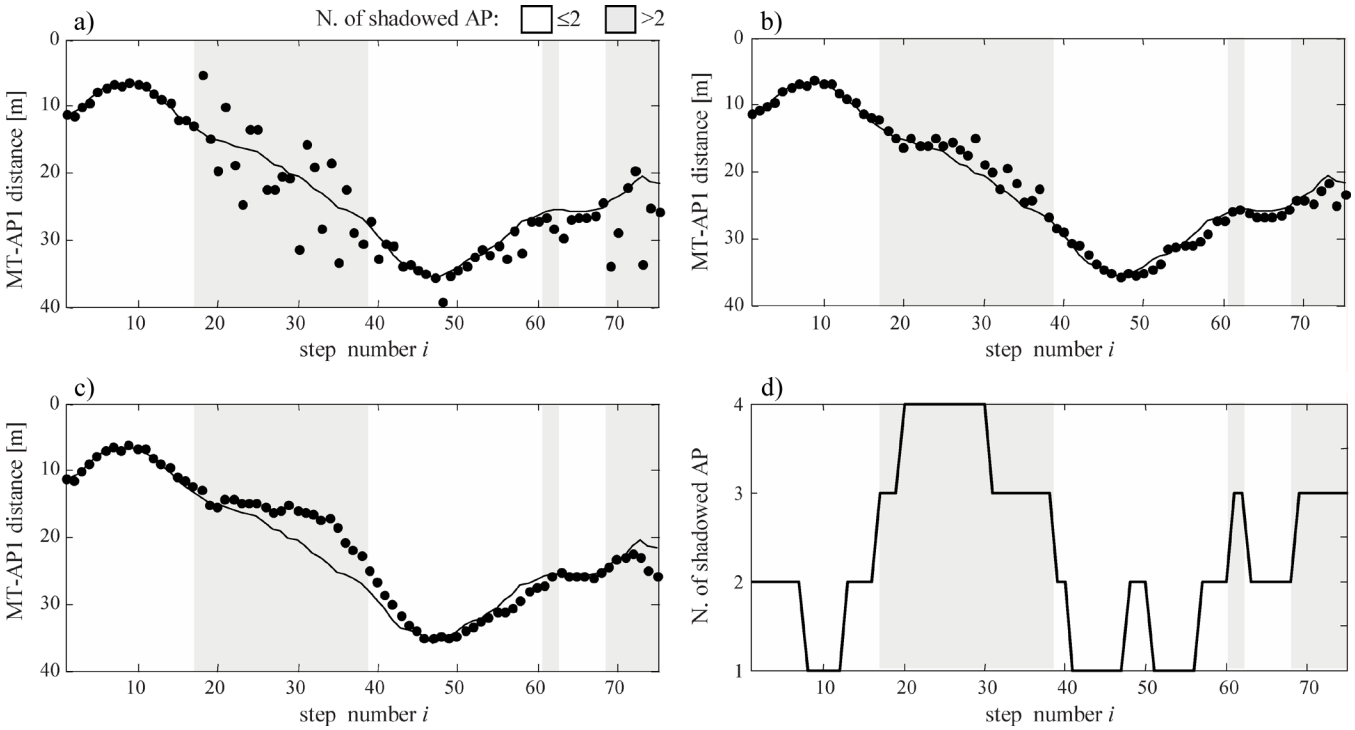

Fig. 5. Ranging performance (for AP1) as a function of the MT position along the path shown in Fig. 3: (a)–(c) MT–AP distance (line) and corresponding estimate (marker) obtained by (a) LML, (b) GF, and (c) PF, respectively; (d) number of shadowed APs.

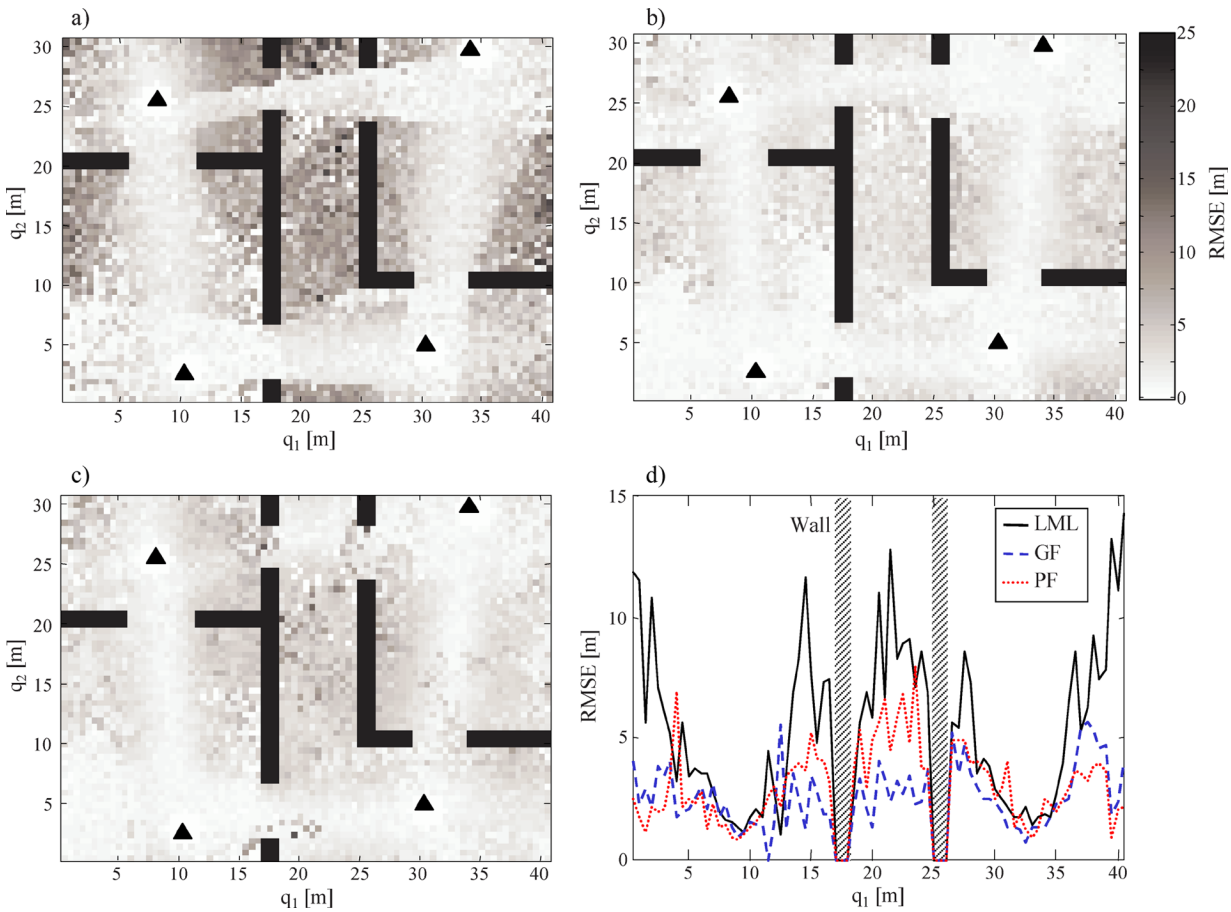

Fig. 6. RMSE of the location estimate as a function of the MT position for (a),(d) LML; (b),(d) GF, and (c),(d) PF . The RMSE is plotted in grayscale as a function of the MT position over the whole 2-D space $\mathcal{Q}$ (a)–(c) and over the 1-D section $\{\mathbf{q} = [q_1, q_2] : q_2 = 15 \text{ m}\}$ (d).

Fig. 6 shows the average localization accuracy evaluated by simulating a longer random walk trajectory composed by $I = 3 \times 10^4$ steps, all around the considered indoor layout. The average performance is computed in terms of root mean-square error (RMSE) of the location estimate as a function of the MT position: for each position $\mathbf{q}_i \in \mathcal{Q}$, the RMSE is obtained as $\text{RMSE}(\mathbf{q}_i) = [\sum_{j \in I(\mathbf{q}_i)} |\mathbf{q}_i - \hat{\mathbf{q}}_i|^2 / |I(\mathbf{q}_i)|]^{1/2}$, where $I(\mathbf{q}_i)$ is the set of all the instants i in which the simulated trajectory flows across $\mathbf{q}_i$ and $|I(\mathbf{q}_i)|$ is its cardinality. In Fig. 6(a)–(c), the RMSE is plotted for (a) LML, (b) GF, and (c) PF using a gray color map to represent the RMSE values. A more detailed view can be found in Fig. 6(d) where the RMSE is shown for the MT positions $\mathbf{q}_i$ restricted along the 1-D section $\{\mathbf{q}_i = [q_{i,1}, q_{i,2}] : q_{i,2} = 15 \text{ m}\}$. The RMSE values in Fig. 6(a)–(d) are quite large due to the poor coverage of the considered scenario. In such a critical condition, the performance of LML turns out to be totally unsatisfactory, while Bayesian tracking still provides acceptable accuracy. As shown in the RMSE map in Fig. 6(a), the LML error is particularly large in poorly covered areas, i.e., outside of the white stripes connecting two APs and in the central corridor where all the APs are in NLOS conditions. On the other hand, both GF and PF [see Fig. 6(b)–(c)] yield a more uniform error map all over the layout (apart from the completely shadowed corridor). The advantage of Bayesian localization in mixed LOS/NLOS conditions can be better appreciated in Fig. 6(d); in the corridor section the LML error ranges from 5 m to 12 m, while the RMSE is around 3 m for GF and 5 m for PF. Please note also that *a priori* information on the topology of the layout (e.g., the positions of walls) is not used here for tracking, but it could be exploited to increase the localization accuracy.

As far as the computational complexity of the tracking example of Fig. 6 is concerned, we recall that the complexity required by the estimate of each MT position is linearly related to the number of grid samples or particles, i.e., $\mathcal{O}(N_g)$ for GF or $\mathcal{O}(N_p)$ for PF tracking. This means that PF localization has a complexity approximately two orders of magnitude smaller than that of GF tracking, but still it preserves almost the same localization accuracy. The RMSE of PF and GF are indeed comparable over the whole layout, apart from the corridor area where the PF error is slightly larger due to the complete lack of LOS coverage (that would require a larger number of particles).

Fig. 7 investigates the robustness of the PF method with respect to the uncertainty of sight statistics information. The sensitivity with respect to LOS/NLOS transition probabilities is tested by evaluating the location RMSE when the MT motion takes place in environments characterized by parameters $\{p_0, p_1\}$ and it is tracked using $\{\hat{p}_0, \hat{p}_1\}$, with $\hat{p}_0 \neq p_0$ or $\hat{p}_1 \neq p_1$. Specifically, in Fig. 7(a), we use $\hat{p}_1 = p_1 = 0.5$, $p_0 = \{0.1, 0.5, 0.7, 0.9\}$ for scenario generation and $\hat{p}_0$ ranging from 0 to 1 for localization; in Fig. 7(b), $\hat{p}_0 = p_0 = 0.5$, $p_1 = \{0.1, 0.5, 0.7, 0.9\}$ for scenario generation and $\hat{p}_1$ ranging from 0 to 1 for localization. The other parameters are chosen as in the previous examples. The RMSE for each parameter set is evaluated by averaging the error over ten trajectories of $I = 300$ steps each. Numerical results in Fig. 7 indicate that the localization accuracy reduces for low p_0 or high p_1 (i.e., for high probability of being in NLOS). The optimum choice for $\{\hat{p}_0, \hat{p}_1\}$ is close to the true value $\{p_0, p_1\}$, but the curves are quite flat around the optimum values denoting moderate mismodeling errors. The flatness of the RMSE curves shows that the proposed method is robust enough even in case of nonperfect knowledge

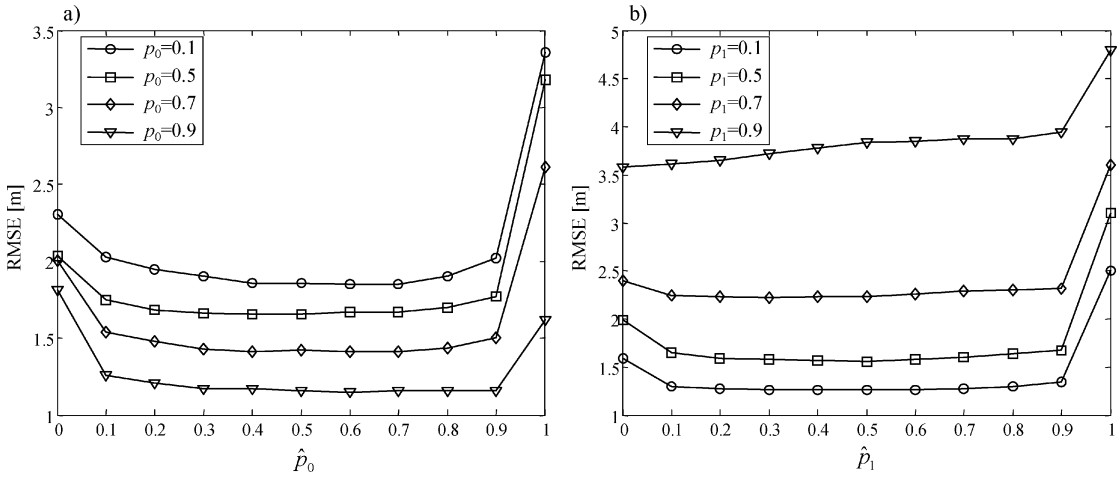

Fig. 7. Sensitivity analysis of the sight parameters for PF localization: (a) sensitivity of the parameter p_0 for $\hat{p}_1 = p_1 = 0.5$; (b) sensitivity of the parameter p_1 for $\hat{p}_0 = p_0 = 0.5$. Symbols $\{p_0, p_1\}$ and $\{\hat{p}_0, \hat{p}_1\}$ denote the parameters used for measurement generation and tracking.

of the sight condition statistics, as good localization performance can be obtained for rough estimates of the model parameters. Furthermore, looking at Fig. 7(a) for $p_0 = 0.1$ and at Fig. 7(b) for $p_1 = 0.9$, it is apparent that for small values of p_0 it is more convenient to overestimate p_0 (i.e., to choose $\hat{p}_0 \geq p_0$), while for large values of p_1 it is more convenient to underestimate p_1 (i.e., to choose $\hat{p}_1 \leq p_1$). This indicates that the performance is optimized when tracking is carried out assuming that the MT stays for long time intervals in LOS and short time intervals in NLOS.

V. Conclusion

A novel Bayesian approach based on PF with JMS modeling has been successfully applied to wireless localization in realistic indoor UWB environments. PDP measurements are used by the Bayesian localization framework to jointly estimate the MT position and its sight conditions with respect to the APs. This approach shows localization performances that are comparable to those of the previously proposed grid-based method without its computational problems. In fact, preliminary results in typical scenarios show that it is possible to obtain the same localization accuracy with computational complexity requirements about 100 times less than the grid-based one. Thereby, such a solution can be considered as a good candidate for real-time terminal-based localization systems.

References

[1] M. Z. Win and R. A. Scholtz, "Ultra-wide bandwidth time-hopping spread-spectrum impulse radio for wireless multiple-access communications," *IEEE Trans. Commun.*, vol. 48, no. 4, pp. 679–691, Apr. 2000.

[2] F. Gustafsson and F. Gunnarsson, "Mobile positioning using wireless networks," *IEEE Signal Process. Mag. (Special Edition on Positioning in Wireless Networks)*, vol. 22, no. 4, pp. 41–53, Jul. 2005.

[3] N. Patwari, J. N. Ash, S. Kyperountas, A. O. Hero, III, R. L. Moses, and N. S. Correal, "Locating the nodes," *IEEE Signal Process. Mag. (Special Edition on Positioning in Wireless Networks)*, vol. 22, no. 4, pp. 54–69, Jul. 2005.

[4] J.-Y. Lee and R. A. Scholtz, "Ranging in a dense multipath environment using an UWB radio link," *IEEE J. Sel. Areas Commun.*, vol. 20, no. 9, pp. 1677–1681, Dec. 2002.

[5] S. Gezici, Z. Thian, G. B. Giannakis, H. Kobayashi, A. F. Molisch, H. V. Poor, and Z. Sahinoglu, "Localization via ultra-wideband radios," *IEEE Signal Process. Mag. (Special Edition on Positioning in Wireless Networks)*, vol. 22, no. 4, pp. 70–84, Jul. 2005.

[6] C. Morelli, M. Nicoli, V. Rampa, and U. Spagnolini, "Hidden Markov models for radio localization in mixed LOS/NLOS conditions," *IEEE Trans. Signal Process.*, vol. 55, no. 4, pp. 1525–1542, Apr. 2007.

[7] A. Logothetis and V. Krishnamurthy, "Expectation maximization algorithms for MAP estimation of jump Markov linear systems," *IEEE Trans. Signal Process.*, vol. 47, no. 8, pp. 2139–2156, Aug. 1999.

[8] M. S. Arulampalam, S. Maskell, N. Gordon , and T. Clapp, "A tutorial on particle filters for online nonlinear/non-Gaussian Bayesian tracking," *IEEE Trans. Signal Process.*, vol. 50, no. 2, pp. 174–188, Feb. 2002.

[9] C. Morelli, M. Nicoli, V. Rampa, U. Spagnolini, and C. Alippi, "Particle filters for RSS-based localization in wireless sensor networks: An experimental study," in *IEEE Proc. (Int. Conf. Acoustics, Speech, Signal Processing (ICASSP)*, May 2006, vol. 4, pp. 957–960.

[10] C. Andrieu, M. Davy, and A. Doucet, "Efficient particle filtering for jump Markov systems. Application to time-varying autoregressions," *IEEE Trans. Signal Process.*, vol. 51, no. 7, pp. 1762–1770, Jul. 2003.

[11] H. Driessen and Y. Boers, "Efficient particle filter for jump Markov nonlinear system," *Proc. Inst. Elect. Eng.—Radar, Sonar, Nav.*, vol. 152, no. 5, pp. 323–326, Oct. 2005.

[12] L. J. Greenstein, V. Erceg, Y. S. Yeh, and M. V. Clark, "A new path-gain delay spread propagation model for digital cellular channels," *IEEE Trans. Veh. Technol.*, vol. 46, no. 2, pp. 477–484, May 1997.